

---

# The Effects of Reduced-Gravity on Planetary Rover Mobility

Journal Title  
XX(X):1–16  
©The Author(s) 2019  
Reprints and permission:  
sagepub.co.uk/journalsPermissions.nav  
DOI: 10.1177/ToBeAssigned  
www.sagepub.com/

SAGE

Parna Niksirat<sup>1</sup>, Adriana Daca<sup>1</sup>, and Krzysztof Skonieczny<sup>1</sup>

## Abstract

One of the major challenges faced by planetary exploration rovers today is the negotiation of difficult terrain, such as fine granular regolith commonly found on the Moon and Mars. Current testing methods on Earth fail to account for the effect of reduced-gravity on the soil itself. This work characterizes the effects of reduced-gravity on wheel-soil interactions between an ExoMars rover wheel prototype and a martian soil simulant aboard parabolic flights producing effective martian and lunar gravitational accelerations. These experiments are the first to collect wheel-soil interaction imagery and Force/Torque sensor data alongside wheel sinkage data. Results from reduced-gravity flights are compared to on-ground experiments with all parameters equal, including wheel load, such that the only difference between the experiments is the effect of gravity on the soil itself. In lunar-g, a statistically significant average reduction in traction of 20% is observed compared to 1-g, and in martian-g an average traction reduction of 5-10% is observed. Subsurface soil imaging shows that soil mobilization increases as gravity decreases, suggesting a deterioration in soil strength which could be the cause of the reduction in traction. Statistically significant increases in wheel sinkage in both martian-g and lunar-g provide additional evidence for decreased soil strength. All of these observations – decreased traction, increased soil mobilization, and increased sinkage – hinder a rover's ability to drive, and should be taken into consideration when interpreting results from reduced-load mobility tests conducted on Earth.

## Keywords

Planetary rovers, reduced-gravity, wheel-soil interactions, terramechanics, parabolic flights, mobility, traction

## Introduction

The Global Exploration Roadmap (International Space Exploration Coordination Group 2018) identifies Mars, the Moon, and asteroids as priority destinations for space exploration. The terrains of Mars and the Moon consist of fine granular regolith with embedded rocks, as do those of a recently discovered class of “rubble-pile” asteroids (Fujiwara et al. 2006; Rozitis et al. 2014). Understanding the nature of interactions with granular terrains is thus crucial to exploring these high priority destinations.

The Mars rovers Spirit, Opportunity, and Curiosity have all experienced mobility challenges stemming from wheel-soil interactions. Spirit had experienced high slippage when crossing loose sandy terrains and ultimately its mission ended after it became embedded in a sulfate sand-filled crater (Arvidson et al. 2010). Opportunity experienced high wheel sinkage and slippage on multiple occasions when traversing sandy crater walls or wind-blown ripples. In some instances wheel slip approached 100%, leading

to scenarios where the rover could not reach the desired traverse target and was forced to re-route (Arvidson et al. 2011). The most significant difficulty for Opportunity was the embedding event in what was dubbed “Purgatory Dune” that lasted from Sol 446 to Sol 484. In total, Opportunity lost more than six weeks of progress while engineers focused on extrication from embedding events. Curiosity has also experienced mobility difficulties when traveling over loose, wind-deposited soil, with the most extreme slippage events occurring when the rover attempted to travel over shallow slope formations (“ripples”). More specifically, Curiosity has experienced high wheel slip events (up to 77% slip) on sols 672 and 709-711 during travel into the Hidden Valley ripple formation (Arvidson et al. 2017).

---

<sup>1</sup>Concordia University, Department of Electrical and Computer Engineering

### Corresponding author:

Krzysztof Skonieczny

Email: kskoniecz@encs.concordia.ca

It is commonplace to perform mobility field tests for Mars rovers with reduced-mass engineering models to mimic the wheel loads that will be experienced in the reduced gravity of Mars. For example, SSTB-lite and Scarecrow are 3/8 mass versions of the Mars Exploration Rovers (Opportunity and Spirit) and Mars Science Laboratory rover (Curiosity), respectively (Lindemann and Voorhees 2005; Heverly et al. 2013). Although these tests correctly capture the effect of reduced gravity (and thus weight) on wheel loads, they do not capture the effect that gravity has on the granular material itself. During efforts to extricate Spirit, this may have contributed to the fact that maneuvers that were successful in on-ground (equivalent wheel load) testing did not ultimately translate into success on Mars (Callas 2015). Less directly, one can also compare slip-vs-slope data reported from Curiosity rover data (Rothrock et al. 2016) to that collected with Scarecrow in analogue field tests (Heverly et al. 2013) and see that on Mars the rover slip tends to be both higher and more highly variable than Earth-based results at equivalent slope (and equivalent wheel loads, as explained above). Earth-based field tests undoubtedly provide useful insight regarding a rover's mobility and guidance, navigation, & control capabilities, but it is important to be able to estimate how much error is introduced in such tests by the fact that the effects of gravity on soil are ignored (Jet Propulsion Laboratory, California Institute of Technology 2009).

Classical wheel-terrain interaction models used in the literature are unable to sufficiently predict the effects of reduced gravity on rover performance. The founding modeling paradigm of terramechanics (the study of vehicle-terrain interactions) relies on simple one-dimensional pressure sinkage relationships to estimate compaction resistance (Bekker 1956) and/or empirical parameters, *e.g.* to estimate the location of maximum pressure beneath a wheel (Wong and Reece 1967). For rigid wheels on dry granular soil – a typical case for planetary rovers – the data shows more complexity than captured by these assumptions; Wong (1967) observed flowing granular soil, and pressure distributions more complex than predicted by one-dimensional compaction.

Empirical parameters in terramechanics models can pose difficulties when extrapolating to new conditions, such as extraterrestrial regolith and gravity. For example, to account for results of wheel traction experiments in reduced-g flights by Kobayashi et al. (2010) within the pressure-sinkage paradigm, a pressure-sinkage coefficient proportional to gravity has been hypothesized by Wong (2012). However, pressure-sinkage coefficients can be directly extracted from data of yet another set of reduced-g flight experiments by Bui

et al. (2009), and are in fact constant across measurements at 1-g, 1/2-g, or 1/6-g.

This inability to reconcile classical terramechanics theory with all available experimental data suggests a need to rethink model assumptions and develop new models for planetary rover-soil interactions. Several researchers today highlight the insufficient predictive power of classical terramechanics models for planetary rovers (Meirion-Griffith and Spenko 2011; Ding et al. 2015; Irani et al. 2011; Senatore and Iagnemma 2014).

A state-of-the-art direction of current terrain interaction research is the discrete element method (DEM), which simulates contact mechanics for millions of individual granular particles. This approach demonstrates promise in modeling planetary rover interactions (Knuth et al. 2012; Slonaker et al. 2017), and is able to set the gravity acting on the soil as a parameter. A novel technique has also been developed using elasto-plasticity theory based descriptions of the wheel-soil interaction (Azimi et al. 2013). This provides a computationally efficient representation that is fully compatible with dynamic models of rovers. Efforts are underway to incorporate the effects of gravity into such models (Ghotbi et al. 2018). As with any new modeling and simulation techniques, or with the application of existing techniques to new problems (in this case, simulating the effects of gravity on wheel-soil interactions), the predictions made will need to be validated against new experimental data.

Preliminary efforts have also been made to account for effects of gravity, at least indirectly, through simulant design. Oravec et al. (2010) designed GRC-1 to produce cone penetrometer readings comparable to those collected on the Moon (*i.e.* in lunar gravity) during Apollo. Edwards et al. (2017) characterized Fillite, a lightweight granular material consisting of hollow micro-spheres, as a possible Martian simulant due to its weight density (weight per unit volume) in Earth gravity being close to the weight density of sand in Martian gravity. As with the new modeling and simulation efforts, predictions made by using these novel simulants also need to be validated against new experimental data.

Flights aboard aircraft flying parabolic arcs are the best opportunity to achieve significant stretches of effectively reduced gravity in a controlled fashion without actually traveling to extraterrestrial surfaces. Only a single dataset has been described in the literature, by Kobayashi et al. (2010), for wheels driving in soil during reduced-g flights. This dataset is based on a self-propelled wheel driving in FJS-1 lunar soil simulant and in Toyoura sand in a wide

range of gravity conditions: 1/6-g, 1/2-g, 3/4-g, 1-g, and 2-g. The data collected includes horizontal travel distance, vertical sinkage, and wheel torque. The data is contrasted to a dataset collected in 1-g that is corresponding but with varying vertical load on the wheel (*i.e.* 1/6 W, 1/2 W, etc.). The difference between the experimental conditions in the two datasets is the effect of gravity on the soil particles themselves. Kobayashi's key observation is that wheel travel is impaired when both the wheel and soil are in reduced gravity, rather than improving as it does when just the load on the wheel is reduced. Kobayashi's experiment provides evidence that adjusting the wheel loading on ground doesn't capture the mobility performance in partial gravity. Additionally, reduced-gravity flights studying excavation (Boles et al. 1997) and bearing capacity (Bui et al. 2009) have similarly produced non-trivial, non-intuitive results that provide further motivation to study rover-soil interactions in reduced gravity. Reduced-gravity flights specifically measuring soil parameters including peak friction angle, residual friction angle, and angle of repose (Alshibli et al. 2003; Kleinhans et al. 2011; Marshall et al. 2018) have yet to arrive at a comprehensive consensus on how gravity affects these parameters.

The contributions of this work fall into two categories: the data collected and the new implications that can be derived from the analysis of that data. With only one prior example of reduced-gravity wheel-soil experiments in the literature, the publication of another – larger – dataset more than doubles the amount of published data of any kind for this research problem. Further, this work includes not only the kind of data previously published but also is the first to collect Force/Torque (F/T) data to explicitly measure net traction and the first to collect subsurface wheel-soil interaction imagery in reduced gravity. These extensive and multi-modal data are particularly valuable for developing future models or simulants to replicate reduced-gravity wheel-soil interactions.

In this work, lunar-g experiments show a statistically significant 20% average reduction in traction compared to corresponding experiments in 1-g with all test parameters (including wheel load) equal, aside from the effect of gravity on the soil. Martian-g results suggest a 5%-10% average reduction in traction. This quantitative analysis has important implications regarding factors of safety that should be considered when interpreting reduced-load mobility tests in Earth gravity on soils similar to those expected extra-terrestrially. Further, the subsurface soil imaging shows the amount of soil mobilized by wheel-soil interaction increases as gravity decreases. This suggests a deterioration in soil

strength which could be the cause for the observed reduction in traction.

Although the improvement of terramechanics models has been mentioned as a motivating factor for this work, the development of new models is beyond the scope of this particular paper which focuses on the experimental results. Another forthcoming publication proposes improved terramechanics modeling that takes into account the velocity profile of the soil under the wheel, wheel flexibility, dynamic sinkage, and gravity. The increase in soil mobilization that is observed in the velocity profile in reduced gravity can be modeled as an effective reduction in the ratio of shear deformation to shear deformation modulus (*i.e.*  $j/K$  at a given slip) to explain the reduction in tractive thrust.

This article is organized as follows: the next two sections describe the experimental setup, parameter settings, and data analysis, to provide sufficient context for the data collected. Next, results are presented, with a focus on the traction and wheel-soil interaction imaging data, which as mentioned above are key contributions of this work. Finally, discussion, conclusions, and future work are presented.

## Experimental Setup

This section describes the main components of the experimental apparatus, including the automated robotic gantry, the wheel, and the soil.

### *Automated test apparatus*

A specialized robotic test apparatus was developed to meet the constraints imposed by reduced-g parabolic flights. During traction tests, the rover wheel is driven (via synchronized control of a horizontal linear actuator and a wheel motor) in an instrumented sandbox that collects pertinent data. A vertical load is applied to the wheel while allowing free vertical motion. Data collection includes net traction force (a.k.a. “drawbar pull”), vertical wheel displacement, and motor current. The wheel is located against a transparent window in the sandbox, and a high-speed camera observes wheel-soil interactions through this window. The apparatus performs automated soil preparation involving loosening, leveling, and compacting the soil to a repeatable state.

The main experiment subsystem is shown in Figure 1, with key elements identified. The wheel axis is driven by a Maxon RE35 motor and MaxPos 50/5 driver. The horizontal motion (along X as defined in the figure) utilizes a Macron Dynamics R6S linear actuator driven by a Kollmorgen

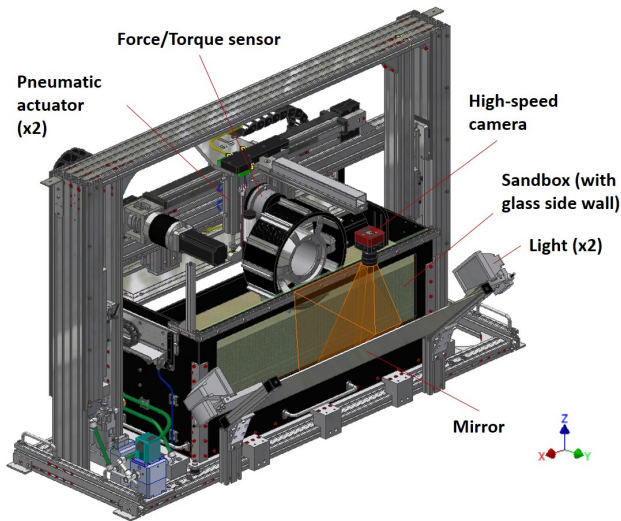


**Figure 1.** Design of automated test apparatus with key functional elements identified.

AKM23C motor and AKD-P00306 driver. These two axis motions are coordinated using a Trio MC4N ECAT.

To both enable the automatic setting of vertical (Z) wheel load and eliminate the need for bulky dead weight components, vertical wheel loading is controlled via a pair of pneumatic cylinders and an Equilibar QB4 digital pressure regulator, with a time constant on the order of 100 ms.

F/T data is collected using an ATI Delta IP60 with a National Instruments USB-6210 data acquisition system. Vertical (Z) wheel displacement is measured using a 100 mm ALPS 10 kOhm slide potentiometer. Images are captured using an IO Industries Flare 4MP monochrome camera with 16 mm EFL f/1.4 lens and Core2 digital video recorder. The camera observes soil motion through a glass sidewall in the sandbox via a mirror tilted at 45 degrees, for the sake of system compactness and vibration reduction. The images are captured, processed, and analyzed using the Soil Optical Flow Technique (SOFT) (Skonieczny et al. 2014).

## Wheel

These experiments studied the performance of a prototype wheel, designed and developed by MDA, for the European Space Agency (ESA) ExoMars mission. The ExoMars wheel has a unique flexible wheel design consisting of a high-strength stainless steel sheet metal rim with two sets of leaf-springs for impact energy absorption (note that the leaf springs cause periodically varying stiffness as the wheel rotates). The ExoMars compliant wheel prototype is 285 mm in diameter and 120.8 mm in width with 12 grousers (Figure 2). Predicting the performance of the wheel depends on empirical data, so there is great value in

conducting experiments, especially in reduced gravity as will be encountered on Mars.



**Figure 2.** A prototype of the ExoMars flexible wheel.

## Soil

ES-2 was selected as the soil for reduced-gravity testing. It is relevant to Martian roving missions, being representative of soils found in many areas of Mars (e.g. between sand dunes). It is characterized as a very fine sand with particle sizes between 30 and 125 microns (Brunskill et al. 2011).

In soil mechanics, the macroscopic properties that characterize the shear strength of a soil are cohesion and internal friction angle. Cohesion in dry soils results from electrostatic bonds and/or interlocking between the soil particles, and is measured as the shear strength when the compressive stresses are equal to zero. The friction angle can be visualized as the angle between the normal force and the resultant force at the time of soil failure in response to a shear stress.

Internal friction angle and cohesion depend on the density of the soil. Brunskill et al. (2011) characterized the Martian simulant ES-2, where the results for the ES-2 direct shear tests show that the instantaneous and effective friction angles are similar in all densities (approximately  $37^\circ$  to  $42^\circ$ ). This would suggest the material is expected to have low cohesion. ESA recommends a density of  $1450 \pm 25 \text{ kg/m}^3$  that emulates a strength which is representative of the soil strength corresponding most to common occurrence on Mars.

It is important to note that low-density regolith is the most challenging to traverse for rovers. It was loose low-density regolith that trapped the NASA rover Spirit. Accordingly, ES-2 simulant is prepared to satisfy the ESA's recommended density, with an interest in targeting the lower end of the density range.

Requirements from ESA were used to select the depth of the soil, ultimately set at 31 cm. There has been research done by ESA-contracted researchers to find the depth at which the floor of the sandbox no longer influences terramechanics experiments for the ExoMars rover wheel

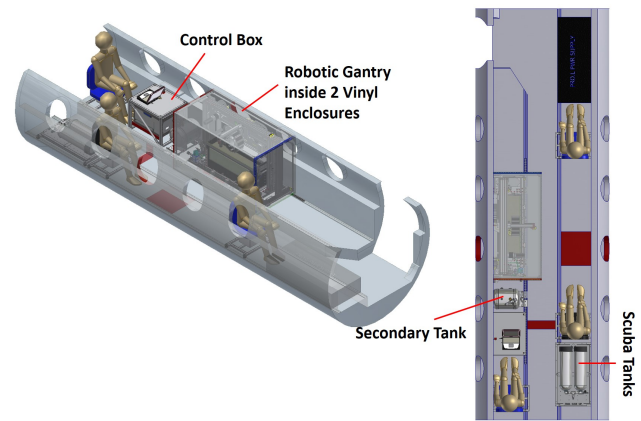
driving in ES-2 simulant. These studies concluded that soil depth greater than 30 cm does not detectably affect the performance while, on the other hand, soil depths less than 25 cm may affect performance. The wheel is located just against – but not rubbing against – the glass sidewall of the sandbox, as is standard practice for imaging wheel-soil interactions (Skonieczny et al. 2014; Senatore and Iagnemma 2014). The sandbox is 90 cm long and 20 cm wide.

In order to ensure repeatable soil conditions, soil preparation procedures including loosening and then compacting and leveling the soil were conducted between each wheel experiment. In recent years, efforts had been made to automate soil preparation (Qian et al. 2013; Lichtenheldt et al. 2017). To achieve automation despite tight in-flight time and space constraints (as seen in Figure 3), a novel rapid automated procedure using pneumatics was developed. The testing and soil preparation were fully automated so that the apparatus could be enclosed to avoid any dust entering the aircraft’s ventilation system. The design and verification of this sub-system is presented by the authors in Skonieczny et al. (2019). ES-2’s very fine particles make it a challenging soil to prepare and work with. Nonetheless, soil height after soil preparation was consistently  $31 \text{ cm} \pm 0.7 \text{ cm}$ ; soil density consistency was shown by the fact that over 80% of cone penetrometer readings within the central 28 cm of the sandbox (covering 100% of the length of the 40% slip and 70% slip tests, and 90% of the length of the 20% slip tests) fell within the 95% confidence bounds determined from a set of reference measurements. Repeatability of soil preparation in flight was demonstrated by the excellent congruency of sinkage and traction data between the three repeats of the 20% slip Martian test (Skonieczny et al. 2019). It should be noted that soil preparation was always conducted during a 1-g preparation phase of flight (between parabolas as shown in Figure 5) for consistency. Further, there was no change in the soil level viewed by the high-speed camera throughout any portion of the flights, suggesting the soil density, once prepared, did not change in reduced gravity.

## Experimental Parameters

The inputs to the system are slip ( $S$ ), wheel loading ( $W$ ) and the effective gravitational acceleration ( $g$ ), as illustrated in Figure 4. The outputs of the system include the measured drawbar pull or net traction ( $F_{DP}$ ), normal force ( $F_N$ ), measured vertical hub displacement ( $z$ ), and high speed images of the wheel-soil interactions.

Additionally, motor velocities and currents are also collected. The velocity from both motors was collected to



(a) Design of the cabin layout for reduced gravity flights.



(b) Inside Falcon 20 cabin.

**Figure 3.** Detailed instrument installation inside the cabin; (a) shows the positioning of the system components within the aircraft cabin and (b) shows the automated terramechanics testing system inside a 2-stage vinyl enclosure (center-left) during reduced-gravity flights.

verify the commanded slip. The angular velocity of the wheel was kept constant at 0.15 rad/s (for a constant  $r\omega$  value of 21 mm/s; see eq. (1)) in all operations. This corresponds to a travel distance of approximately 15 to 50cm, depending on the slip value (since the speed of wheel rotation is held constant, the distance travelled changes based on the slip value). Considering the low speed, it is assumed these experiments correspond to a quasi-static condition. The motor current was used to validate the motor performance and to confirm the F/T sensor data. Motor torque can be estimated for the wheel motor as  $I_{mi} * K_{mi}$ , where  $I_{mi}$  is motor current for motor  $i$ , and  $K_{mi}$  is the torque constant (e.g. 0.029 Nm/A for the wheel motor).

### Input: Slip ( $S$ )

The amount of traction a wheel produces is related to how much it slips (Bekker 1956). A key objective in enhancing the mobility of rovers operating on soft terrain is to reduce the amount of slip for a given task (with its associated required traction). Equivalently, it is desirable to be able to

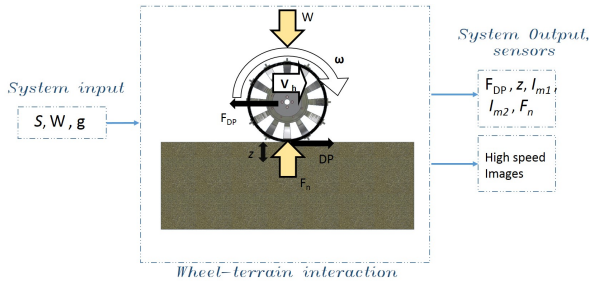


**Figure 4.** Inputs and outputs of the terramechanics experiments.

achieve higher net traction at any given slip. The value of slip is defined as

$$S = \frac{r\omega - V}{r\omega} * 100\% \quad (1)$$

where  $\omega$  and  $V$  are the angular and horizontal wheel velocity, respectively.  $r$  is the original (undeformed) wheel radius measured to the rim; for a flexible wheel (such as ExoMars) if there is a significant deflection along the traverse, there is uncertainty in finding the appropriate radius and calculating the precise slip at any given moment. However, despite the deflection, the circumference of the rim does not change (recall it is steel sheet metal) and over a long enough rotation (by angle  $\Delta\Omega$ , say), the total length of rim rotating past has to approach  $r\Delta\Omega$  or the wheel would come apart. Thus, equation 1, even allowing for wheel deformation, gives the correct slip on average. In this experimentation campaign, slip was varied between 10% and 70%.

### Input: Wheel load ( $W$ )

Wheel load is another parameter that affects traction, and thus rover mobility. In this experimentation campaign two wheel loads are considered: 164 N and 225 N. The wheel load,  $W$ , is the sum of the wheel unit weight and applied force on the wheel unit. In partial gravity, the weight of the wheel unit is lower than on Earth, so for directly comparable tests (*i.e.* at equal total wheel load) this reduction in weight is compensated by an equal and opposite increase in applied pneumatic force (using the pneumatic cylinders and digital pressure regulator described earlier) during the reduced-gravity flights.

It should be noted that due to various factors, including the wheel's grousers and suspension springs and the time constant of the pneumatic pressure regulator, the wheel load is not exactly constant throughout a test and is instead a

periodic signal. However, the signal is consistent across tests and the average load equals the setting described above.

### Input: Effective gravity ( $g$ )

The experimental apparatus described above flew aboard Canada's National Research Council's (NRC) Falcon 20 aircraft. As shown in Figure 5, to achieve effective partial gravity, the aircraft produces ascent and descent flight maneuvers. During each parabola, a partial gravity environment is maintained for approximately 20 – 30 seconds between two 2-g maneuvers. During the flight, three components of acceleration, longitudinal ( $A_x$ ), lateral ( $A_y$ ), and vertical ( $A_z$ ) were measured with an inertial measurement unit (IMU) fixed inside the plane. Figure 5 shows that accelerations in the lateral and longitudinal directions are almost zero during partial gravity, indicating that it is unnecessary to take the effects of the accelerations in directions other than  $A_z$  into consideration. In total, 10 martian-g parabolas and 7 lunar-g parabolas were flown with the wheel testing apparatus.

Recall that because the applied pneumatic force is adjusted to compensate for any effects of gravity on the wheel unit weight, wheel load can be controlled to be equivalent across tests. Thus, the effect of gravity on the soil itself is isolated in the experimental campaign.

Table 1 summarizes the tests conducted in this experimentation campaign.

**Table 1.** Number of experiments completed at each combination of parameter settings. All tests conducted in ES-2 (density of  $1450 \pm 25$  kg/m), with  $\omega = 0.15$  rad/s.

Slip (%)	Wheel Load (N)	Number of Tests		
		1-g	Martian-g	Lunar-g
10	164	1	1	1
20	164	3	3	2
30	164	1	1	1
40	164	1	1	1
70	164	1	1	1
10	225	1	1	0
20	225	1	1	0
30	225	1	1	0

### Output: Drawbar Pull ( $F_{DP}$ )

Drawbar pull (DP) is a crucial parameter in evaluating the performance of rover wheels, as it indicates the ability of the rover to pull/push itself in the desired direction of motion. DP is the difference between the thrust force ( $T$ ) and the sum of resisting forces ( $\Sigma R$ ) acting on the rover as expressed in equation (2). In this work we use DP to refer to drawbar pull

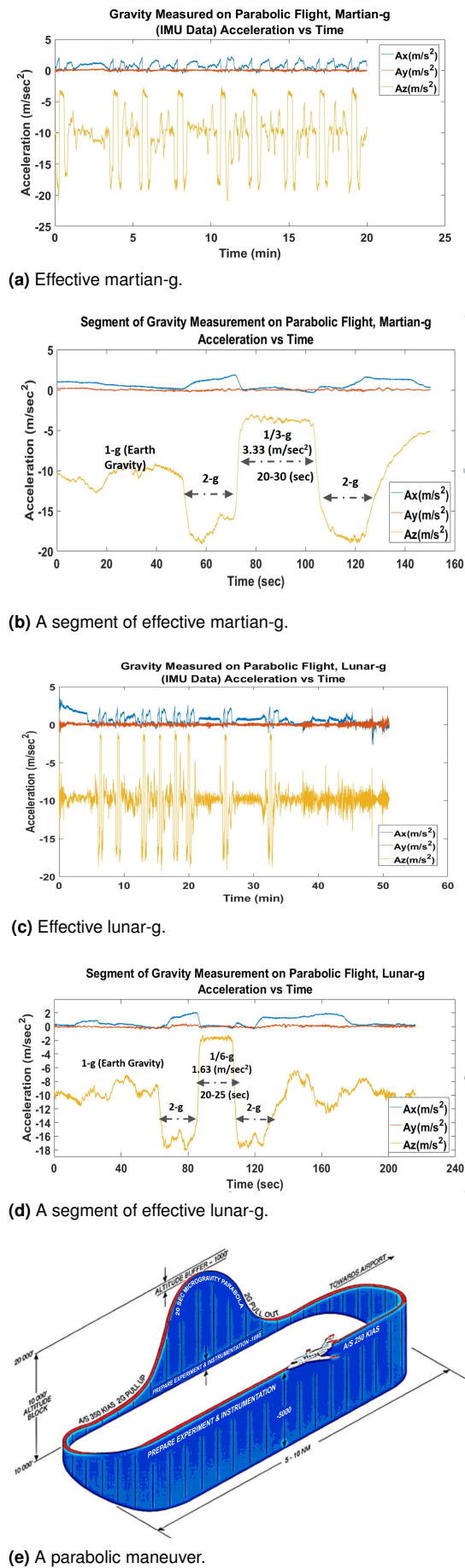


**Figure 5.** Parabolic flights: (a) martian-g flight with zoom-in (b) on one parabola; (c) lunar-g flight with zoom-in (d) on one parabola; (e) partial gravity flight trajectory including a reduced-g parabola as well as an experiment and instrumentation preparation phase between parabolas.

Prepared using sagej.cls

in general, and  $F_{DP}$  to refer to our measurement of drawbar pull.

DP is the net external force that a vehicle can generate, which can also be related to slope climbing ability (Bekker 1956), and as such, DP is commonly used to predict a vehicle's slope-climbing performance (Freitag et al. 1970). Therefore, DP is chosen here as the metric for evaluating the performance of the wheel and predicting the maximum slope that the rover can climb at each slip rate (see Figure 6b and equation (3)). DP/W is approximately constant for different loads, W, within a wheel's practical operating range (Freitag et al. 1970). The component of wheel load perpendicular to the slope is reduced to  $W \cos(\theta)$ , with a corresponding reduction in DP relative to flat ground. This remaining  $DP_\theta$  ( $=DP_0 \cos\theta$ ) must then balance the component of load acting parallel to the slope (i.e.  $W \sin\theta$ ).

In this experimentation campaign, the F/T sensor connected to the wheel unit gives a measurement of drawbar pull, i.e.  $F_{DP}$ , during slip-controlled traverses.

$$DP = T - \sum R \quad (2)$$

$$\theta_{max} = \tan^{-1}(DP/W) \quad (3)$$

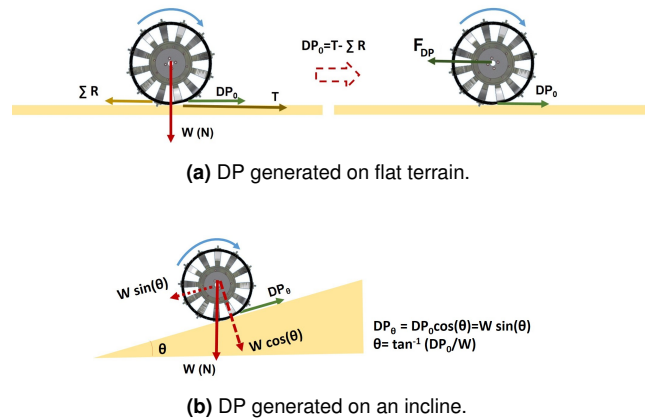


**Figure 6.** DP generated at each slip rate can be used to estimate maximum climbing angle at that particular slip. (a) DP generated is balanced by a reaction force, sensed by force torque sensor ( $F_{DP}$ ), (b) DP generated on inclination is balanced by gravitational resistance (i.e.  $W \sin(\theta)$ )

### Processing of drawbar pull data

$F_{DP}$  measurements were averaged for each slip test and divided by average wheel load (W). The drawbar pull-weight ratio (DP/W) is a commonly used metric in the field of terramechanics that refers to the load a vehicle can tow relative to its own weight, or vertical load, and can also be related to its slope-climbing ability as discussed earlier. In these experiments, due to the wheel's grousers and

suspension springs (and possibly other system dynamics), the drawbar pull and wheel load data exhibit a periodic pattern, which has previously been observed by Irani et al. (2014) in wheels with and without grousers. Consequently, the data used for averaging had to be selected systematically in order to facilitate meaningful comparisons between the tests. The approach was to analyze exactly two periods of data, and always at the same stage of the test. This was done by first identifying the start of motion,  $t_0$ , in each test. Then  $t_1$ , the length of time between the start of motion and the beginning of the averaging window, was selected such that the transients at the beginning and end of the test were not included in the average calculation (*i.e.* such that the quasi-steady state condition was achieved, as determined by qualitatively observing the data). Finally  $t_2$ , the length of the averaging window, was defined to encompass two periods of oscillation, which is 14 s out of the 20-25 s of wheel motion (since the periodicity of the data was found to correspond to the geometry of the wheel, and the rotational speed was constant for all tests, the period is the same for each test). Only  $t_0$  differed between tests;  $t_1$  and  $t_2$  were the same for all tests. These time segments are demarcated in Figure 7, which shows two examples of DP and W data from 10% and 20% slip tests in martian-g with wheel load setpoints of 225N. At low slip values a true quasi-steady state is achieved; as can be seen in Figure 7, the maximum and minimum values of drawbar pull are similar for each period. At higher slip values a true steady-state cannot be achieved in under 20 s, but nonetheless relative comparisons of DP (and sinkage) between different gravity levels are still valid because using the same  $t_1$  and  $t_2$  ensures the data is from equivalent phases of the motion.

### Output: Sinkage ( $z$ )

Wheel sinkage is a measure of the response of the terrain to a specific loading, and affects wheel performance. Sinkage is a function of slip. In this experimental campaign, sinkage is estimated from the vertical hub displacement of the wheel as measured by a potentiometer attached to the wheel unit. The wheel hub displaces vertically due to sinkage but also due to wheel deflection. Average wheel deflection is assumed to stay constant throughout any given test with constant wheel loading.

At equal soil strength, higher sinkage generates higher resistive forces. On the other hand, at equal sinkage, a soil with higher strength generates higher resistive forces. Any variation in resistive forces can be attributed to sinkage and/or soil strength. These resistive forces act against the thrust, and therefore contribute to a reduction of DP.

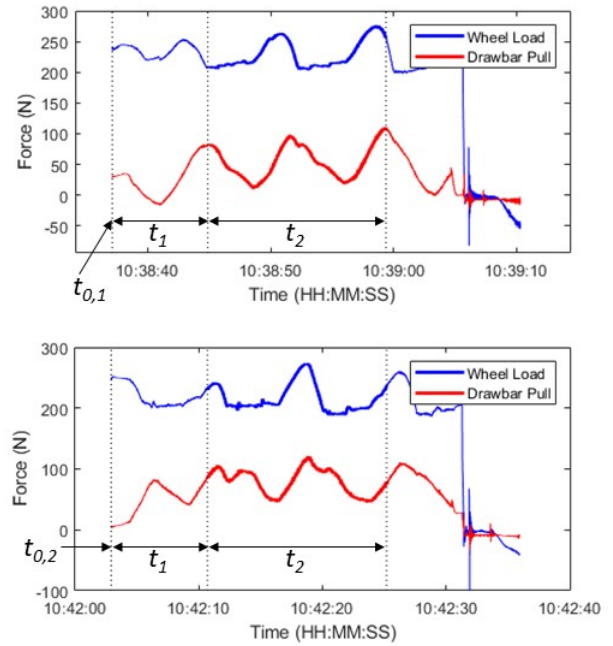


**Figure 7.** Examples of periodic drawbar pull and wheel load data from the 10% (top) and 20% (bottom) slip tests in martian-g with wheel load setpoints of 225N.  $t_0$  marks the start of motion (data prior to  $t_0$  are not shown here),  $t_1$  is the time between  $t_0$  and the beginning of the averaging window, and  $t_2$  is the length of the averaging window (two periods of oscillation). Bolded lines show segments of data used for averaging.

### Processing of sinkage data

The raw  $z$  measurements, when converted to units of mm, represent the distance between the wheel hub and the potentiometer. In order to obtain measurements that represent sinkage relative to the top of the soil (*i.e.* such that a value of 0 mm corresponds to the top of the soil), the distance from the top of the soil to the potentiometer was subtracted from the readings. Furthermore, since the soil height was not perfectly consistent between runs (with a standard deviation of  $\pm 7$  mm), the soil height was measured from each video in order to estimate the distance from the potentiometer to the top of the soil in each test. However, one video was lost (one of the tests in lunar-g at 20% slip), so for this case, the averaged soil height over all the other lunar tests was used.

Example sinkage data is shown in Figure 9.

### Output: Images

Observing how the soil responds to being acted upon by a wheel can generate insight into phenomena governing wheel performance (Skonieczny et al. 2012, 2014). A high-speed camera is used to image the soil in the region where it interfaces with the wheel. The camera is attached to the horizontal axis and moves alongside the wheel capturing the high-resolution image frames of the wheel-soil interaction from the mirror reflection of the testbed's window. In Figure

1, the camera's angle of view and glass sidewall view field are shown in orange.

Two external LED floodlights are placed approximately 1000 mm apart at both ends of the mirror at an angle pointing towards the window, to avoid direct reflection into the camera, providing illumination, high contrast, and reduced shadows along the mirror.

The videos from the wheel-soil interaction experiments were collected in black and white at 37 frames per second (fps). The video was subsequently converted to images where each pixel represents an area of  $0.4 \times 0.4$  mm. A raw image from the testbed is shown in Figure 8, with indications of the direction of the wheel traverse where the rolling wheel is driving counterclockwise and the direction of travel is from the right to the left of the image.

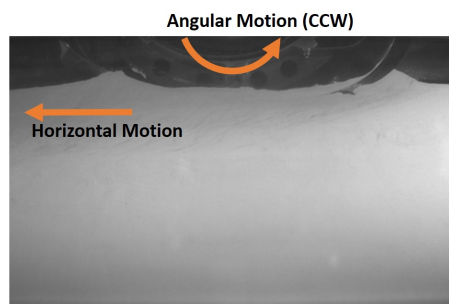


**Figure 8.** Image captured through the glass window of the ExoMars flexible wheel in ES-2 Martian simulant; note camera field of view shown in Fig. 1. This image shows the interface contact patch of the flexible wheel with soil at 70% slip and 164 N wheel loading.

#### Overview of image processing technique

To analyze soil motion observed through the glass sidewall of the sandbox, a dense motion estimation technique called the soil optical flow technique (SOFT) is used, discussed in detail by Skonieczny et al. (2014). This technique calculates motion at each pixel of the image between consecutive images. Two displacement fields are produced, one for horizontal and one for vertical motion, in units of pixels. The parameter settings used for this analysis are shown in Table 2.

**Table 2.** Parameter settings used for SOFT.

Regularization parameter, $\lambda$	0.1
Pyramid levels	3
Spacing of pyramid levels	2
Maximum number of iterations	10

Using this technique, velocity vectors were obtained for each pair of successive frames. Then, these vectors were averaged over time ranges identified from patterns observed in the corresponding sinkage data. This was done to eliminate noise and transients caused by the response to

passing grouzers or minor variations in soil state. Averaging boosts the signal-to-noise ratio for compliant wheels that induce small soil motion and thus depicts smoother flow patterns, portraying more meaningful results in comparison to a single frame pair. Additionally, it was hypothesized that soil motion would be consistent in sections with relatively constant rates of change in sinkage. Examples of sinkage data are shown in Figure 9, with arrows indicating the sections selected for averaging. In Figure 9a, sections 1, 3, and 5 are called 'rises', as the sinkage is rising during these segments. Similarly, sections 2, 4, and 6 are called 'plateaus'. In the lower slip ratio tests, sinkage 'falls' (e.g. sections 1, 5, and 9 in Figure 9b) and 'valleys' (e.g. sections 2, 6, and 10 in Figure 9b) are also observed.

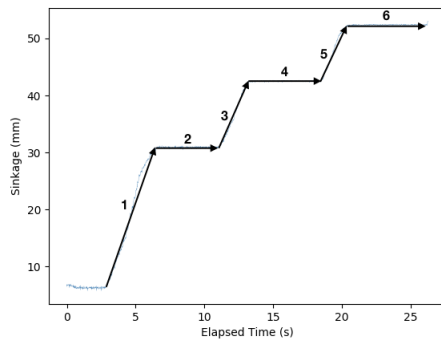
In order to directly compare tests exhibiting only two distinct types of sinkage behaviour ('rises' and 'plateaus', as seen in Figure 9a) to tests where four types of sinkage behaviour were seen ('rises', 'plateaus', 'falls', and 'valleys', as seen in Figure 9b), the sinkage 'plateaus' in the former were divided into three segments. The phenomenon observed in 9b is concurrent with the varying of the wheel's stiffness (depending on leaf-spring positions), and demonstrates the wheel hub recovering vertically when stiffer sections of the wheel interact with the soil at low slip. Sinkage behaviour similar to that shown in Figure 9a tended to occur during higher-slip conditions. At higher slip, the stiffer sections of the wheel dig into and excavate soil (slip-sinkage), overwhelming any possible vertical recovery.

Finally, for the purpose of comparing the average estimated flow fields, the velocity magnitudes at each slip are all normalized with respect to the rim speed. Rim speed is computed as the tangential rim velocity relative to the wheel hub ( $r\omega$ , which is constant across all tests) minus horizontal wheel (and thus hub) velocity (which decreases with increasing slip, but is constant and equal for all tests at a particular slip).

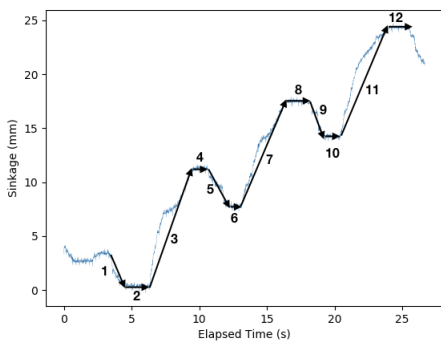
Example SOFT output is shown in Figure 14.

#### Output: Drive motor current

Drive motor current measurements provide insight about the torque required to spin the wheel, or the 'difficulty' with which the motor spins the wheel. Increased motor current is required when soil resistance is higher, which can occur as a result of increased sinkage and/or higher soil strength. It is expected that when comparing two cases with equivalent soil strength and differing sinkage, higher motor current would be seen in the case with higher sinkage. Similarly, in two cases with equal sinkage and different soil strength, motor



(a) Sinkage data for test in martian-g at 70% slip and 164N wheel load.



(b) Sinkage data for test in martian-g at 20% slip and 164N wheel load (Repeat A).

**Figure 9.** Examples of sinkage data with numbered arrows indicating segments used for averaging of the SOFT results.

current would be higher in the case where stronger soil is encountered.

## Results and Discussion

### Experimental error

One source of error in these experiments is the variance remaining after soil preparation. The properties of the soil simulant used, ES-2, are sensitive to soil conditions, as described by Skonieczny et al. (2019), and each time the soil preparation procedure is performed, some error is introduced with a zero mean and a nonzero variance (*i.e.* this error is random, not systematic). Another possible source of error is the variability in gravity level during the flights. Looking at the IMU data from the flights, the gravity levels were not perfectly constant and consistent, as can be seen in the examples shown in Figure 5, but the variations within and between tests are much smaller than between lunar-g, martian-g, and 1-g. Finally, there is also the further difference between reduced-g experiments done in flight and 1-g experiments done in a stable laboratory environment (with a more rigid substrate and less vibration). However, the differences observed between lunar-g and martian-g

results are in themselves substantial and consistent with an interpretation that the 1-g tests are valid for comparison (*i.e.* the differences observed between lunar-g and 1-g are larger than those between martian-g and 1-g, with both differences in the same direction).

### Drawbar pull

Average DP/W versus slip ratio can be seen in Figures 10 and 11 for (i) 164N wheel load tests in 1-g and lunar-g, and (ii) 164N and 225N tests in 1-g and martian-g, respectively. The average ratio of DP/W in reduced-g to 1-g was computed for each case, and a paired, two-tailed t-test was used to determine statistical significance ( $p < 0.05$ ).

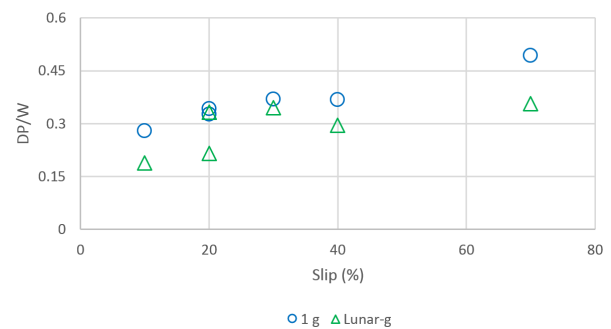


**Figure 10.** Average drawbar pull-wheel load ratio versus slip ratio for tests in 1-g and lunar-g with wheel load setpoint of 164N.

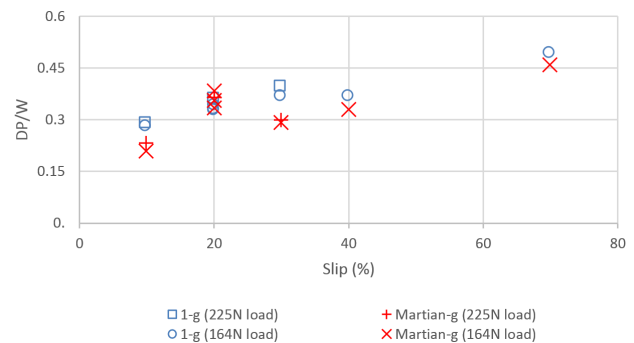


**Figure 11.** Average drawbar pull-weight ratio versus slip ratio for tests in 1-g and martian-g with wheel load setpoints of 164N and 225N.

### Effect of gravity on drawbar pull

DP/W was 20% lower on average in lunar-g compared to 1-g, and the difference between these two datasets was statistically significant ( $p = 0.02$ ). In martian-g, a decrease in DP/W was also detected (6% with 164N wheel load, 14% with 225N wheel load, and 8% if the 164N and 225N datasets are combined), but it was not statistically significant ( $p = 0.30, 0.24, \text{ and } 0.09$  respectively). This can be explained by the fact that

- (i) the statistical degrees of freedom ( $n-1$ ), where  $n$  is the number of data points in the sample, are relatively low in these datasets, resulting in low statistical power of the hypothesis tests; consequently, only relatively large differences are detected as significant,
- (ii) there is some nonzero experimental error, as described above, and
- (iii) the difference between martian-g and 1-g is not as large as the difference between lunar-g and 1-g (since there is a smaller difference in the input signal, gravity, the difference in the output signal, drawbar pull, is also smaller, and thus there is a lower signal-to-noise ratio, resulting in the difference not being statistically significant in this case).

Nevertheless, a decrease in drawbar pull was detected in martian-g, and coupled with the statistically significant decrease observed in lunar-g, this leads to the conclusion that drawbar pull is monotonically related to gravity.

A reduction in drawbar pull is consistent with lower soil strength in reduced gravity.

### Sinkage

Figures 12 and 13 show the maximum sinkage reached during each test (irrespective of number/types of segments observed, see Figure 9) versus slip ratio for tests with, respectively, (i) 164N wheel load in 1-g and lunar-g and (ii) 164N and 225N wheel loads in 1-g and martian-g. Again, paired, two-tailed t-tests were used to determine the statistical significance of the differences observed between the reduced-g and 1-g results.

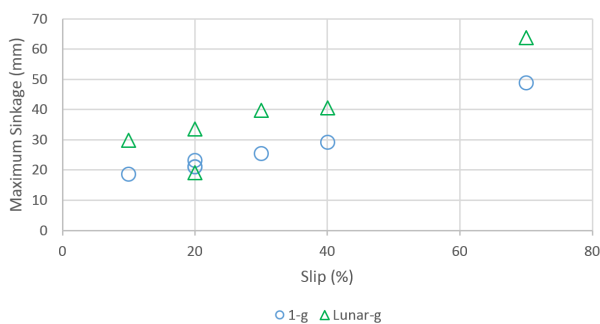


**Figure 12.** Maximum sinkage versus slip ratio for tests in 1-g and lunar-g with wheel load setpoint of 164N.

#### Effect of gravity on sinkage

Maximum sinkage was 38% higher on average in lunar-g compared to 1-g, and this difference was statistically significant ( $p = 0.01$ ). In martian-g, with wheel loads of 164N and 225N, maximum sinkage was 27% and 47% higher than in 1-g, respectively. Both of these differences were found to

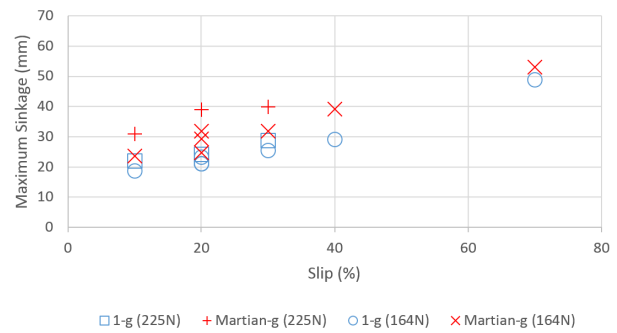


**Figure 13.** Maximum sinkage versus slip ratio for tests in 1-g and martian-g with wheel load setpoints of 164N and 225N.

be statistically significant ( $p = 0.001$  and  $0.02$ , respectively). These results lead to the conclusion that sinkage increases in reduced gravity. Increased sinkage in reduced-g is consistent with reduced soil strength, as bearing capacity (a soil's ability to withstand vertical load without failing) is directly related to soil strength.

#### Effect of gravity on sensitivity to wheel loading

When the wheel load was increased from 164N to 225N (an increase of 37%), maximum sinkage increased by an average of 14% in the 1-g experiments, and in martian-g, maximum sinkage increased by an average of 31%. This difference can be observed visually in Figure 13. This result indicates that sensitivity to wheel loading may also be increased in reduced gravity. This is again consistent with reduced soil strength and thus reduced bearing capacity. In martian-g, sinkage increases almost proportionally to the increase in load, whereas in 1-g the additional sinkage is much less than proportional. In terramechanics, such an effect may suggest a gravity dependent (static and/or dynamic) pressure-sinkage exponent.

#### Image processing

Figures 14, 15, and 16 show visualizations of the magnitude of soil flow velocity for 1-g, martian-g, and lunar-g tests at 70%, 40%, and 20% slip, respectively, and Figure 17 shows the effect of wheel load setpoint on the magnitude of soil flow velocity in 1-g and martian-g. The velocities are normalized with respect to the commanded rim speed such that the color map indicates dark blue as static and dark red as maximum motion (*i.e.* commanded rim speed or higher). Also note that the illumination (by floodlights at both ends of the mirror) sometimes introduces artifacts in the lower corners of the images, so they have been cropped accordingly.

Vector fields for the 70% slip tests are shown in Figure 18. Here, both the magnitude and the direction of soil flow velocity are represented, and the magnitude of the

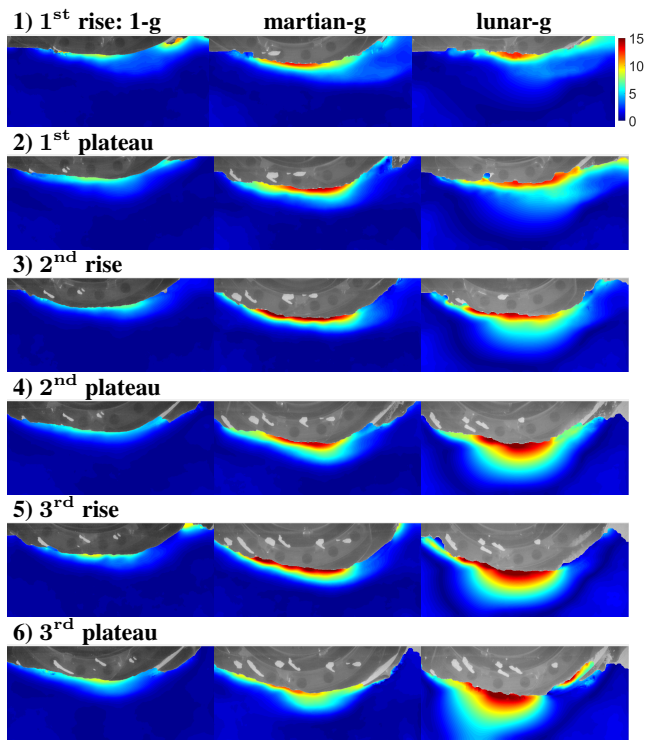


**Figure 14.** Visualizations of magnitude of soil flow velocity for, from left to right, tests in 1-g, martian-g, and lunar-g, at 70% slip and 164N wheel load, averaged over sinkage ‘rise’ and ‘plateau’ segments as demonstrated in Figure 9a. The colorbar indicates velocity in mm/s (with the maximum being commanded rim speed).

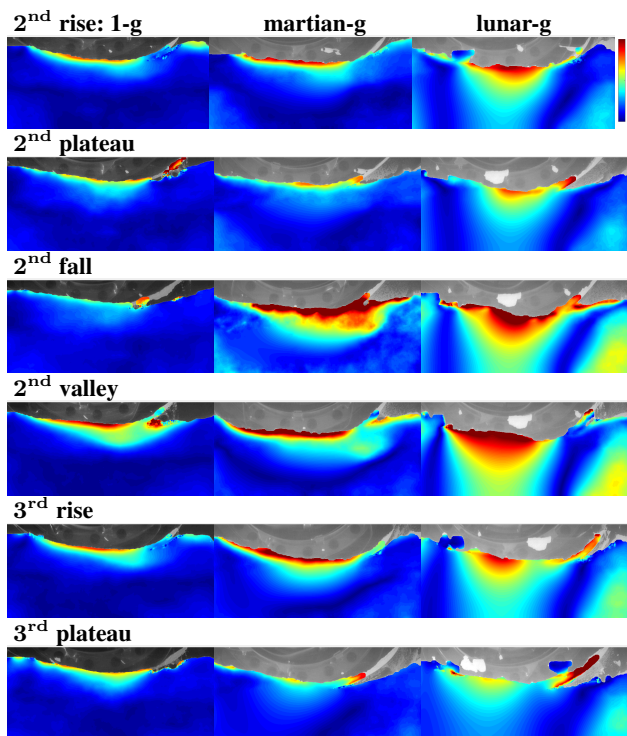


**Figure 15.** Visualizations of magnitude of soil flow velocity for, from left to right, tests in 1-g, martian-g, and lunar-g, at 40% slip and 164N wheel load, averaged over sinkage ‘plateau’, ‘fall’, ‘valley’, and ‘rise’ segments as demonstrated in Figure 9b. The colorbar indicates velocity in mm/s (with the maximum being commanded rim speed).

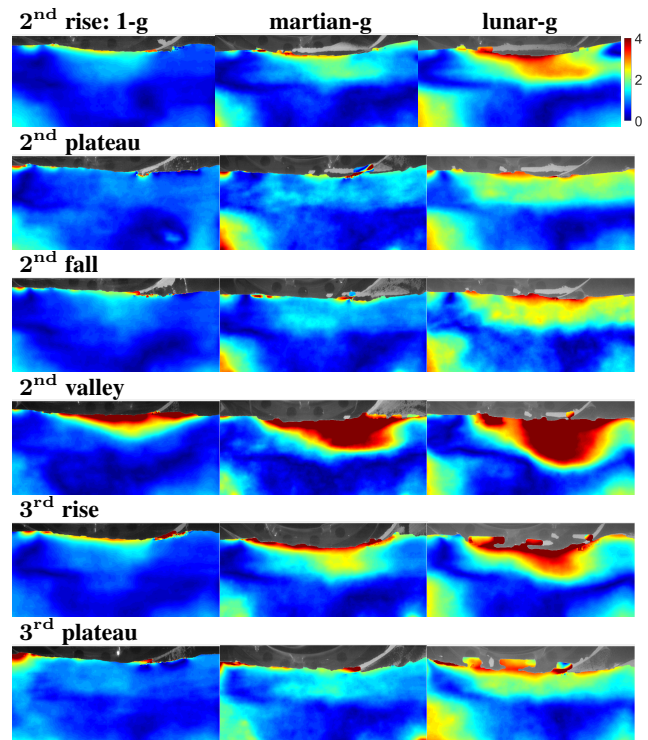


**Figure 16.** Visualizations of magnitude of soil flow velocity for, from left to right, tests in 1-g, martian-g, and lunar-g, at 20% slip and 164N wheel load, averaged over sinkage ‘plateau’, ‘fall’, ‘valley’, and ‘rise’ segments as demonstrated in Figure 9b. The colorbar indicates velocity in mm/s (with the maximum being commanded rim speed).

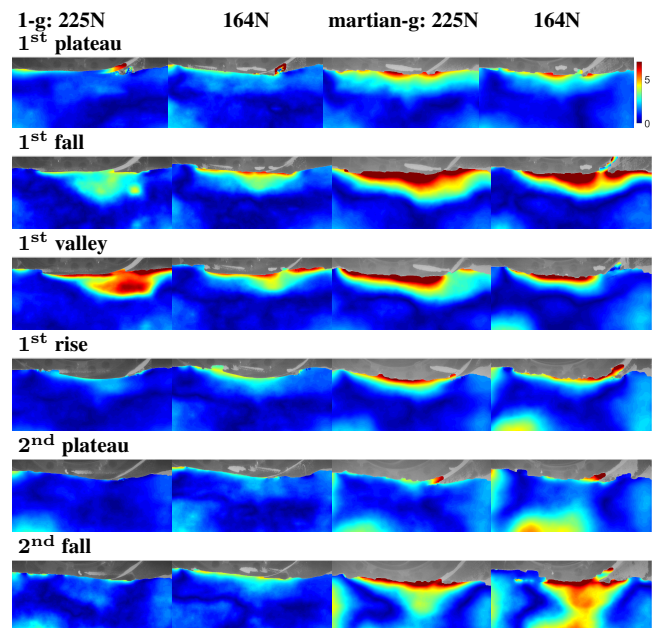


**Figure 17.** Comparison of magnitude of soil flow velocity for tests with wheel load setpoints of 164N and 225N in 1-g and martian-g, at 30% slip. Results are averaged over sinkage ‘plateau’, ‘fall’, ‘valley’, and ‘rise’ segments as demonstrated in Figure 9b. The colorbar indicates velocity in mm/s with the maximum being commanded rim speed.

commanded rim speed is indicated by a reference arrow in the upper right of each plot. Velocity magnitude colormaps

and vector fields for all other tests are provided as a supplementary appendix, as they are too numerous to include here.

#### *Effect of gravity observed in image analysis*

In Figures 14, 15, and 16, looking down a column shows the changes in soil motion with respect to time (averaged according to the sections identified in the sinkage data). Looking across a row compares soil motion in different gravities for a particular section of time in a test.

It is clear that at any time, and at any slip rate, there is more soil motion in partial gravity (martian and/or lunar) than in 1-g. Furthermore, there is notably more soil motion in lunar gravity than in martian gravity. In reduced gravity, shearing forces generated during wheel-soil interaction produce more soil mobilization at any slip rate at equal loading.

In lower gravity, as the wheel traverses forward in time, the regions of mobilized soil become larger and the magnitude of velocity fields increases. On the other hand, the results suggest that in 1-g, the region and magnitude of mobilized soil do not increase over time. In Figures 14 and 18, comparing the column of lunar results with the corresponding column of 1-g results illustrates the time-dependent mobility deterioration in low gravity.

Another observation is that in both 1-g and martian-g, increasing the wheel loading from 164N to 225N does not impact the soil mobilization significantly. Figure 17 illustrates the effect of these variations at 30% slip. From the illustrations, it is clear that the influence of gravity on the soil mobilization is much more prominent than the influence of the normal load.

Furthermore, it was observed that in all 1-g tests, there was significantly more soil motion in the sinkage ‘valleys’ (*i.e.* just before an increase in sinkage). It appears that shear failure of the soil occurs during the ‘valley’ segments, which leads to the subsequent rise in sinkage. It was also noted that in all tests, the cyclical sinkage behaviour corresponded to the position of the wheel’s leaf-springs. In reduced gravity, the experiments at lower slip ratios (*e.g.* 20% slip, as seen in Figure 16) exhibit a similar pattern with the highest amount of soil motion occurring in the ‘valleys’, but at higher slip ratios (*e.g.* at 30% and 40% slip, as seen in Figures 17 and 15, respectively), there is more motion earlier in the cycle (during the sinkage ‘falls’), indicating that soil failure occurs more readily in reduced gravity. There is also more soil motion during the sinkage ‘rise’ segments in reduced gravity, which reveals that increased soil motion continues for a longer period of time after failure.

In summary, gravity has a significant effect on the wheel-soil interaction at equal slip and wheel loading. Moreover, under the influence of lower gravity, these interactions are more variable in time than in 1-g. The greater soil mobilization observed in reduced-g is consistent with reduced soil strength, as more soil motion demonstrates a greater propensity for the soil to fail.

#### *Drive motor current*

Figure 19 shows average drive motor current versus slip for tests in 1-g, martian-g, and lunar-g with 164N wheel load setpoints, and Figure 20 shows average drive motor current versus slip for tests in 1-g and martian-g with 225N wheel load setpoints.

#### *Effect of gravity on drive motor current*

There is no significant difference observed in drive motor current between the effective gravity levels. In the 225N wheel load tests, the average current was slightly lower in martian-g than in 1-g, but this difference was not statistically significant ( $p = 0.097$ ). The lack of difference in motor current is, however, consistent with the differences observed in the corresponding sinkage measurements. Normally, it is expected that more motor current is required when more sinkage is encountered under equivalent soil strength. However, in the reduced-gravity experiments, sinkage increased significantly, but motor current did not. This discrepancy can be attributed to decreased soil strength in lower gravity.

#### *Conclusion*

This work is the first to directly observe rover wheel-soil interactions in reduced gravity, aboard parabolic flights achieving martian and lunar gravitational accelerations. An ExoMars rover prototype wheel was operated against a glass window along the side of a sandbox, and the interactions were visualized using a technique that had been developed by one of the authors. Results are compared to experiments conducted in Earth gravity.

Controlling the wheel slip and wheel load ensures that the only difference between experiments is the effect of gravity on the soil particles themselves. It is important to consider that these differences between experiments are equivalent to the difference between actually driving a rover on Mars and testing a reduced-mass version of the rover (*i.e.* with equal wheel normal load) in similar soil on Earth.

Optical flow-based visualization of the soil motion (imaged with a high-speed camera) shows that more soil is mobilized by the wheel in reduced gravity. More soil motion

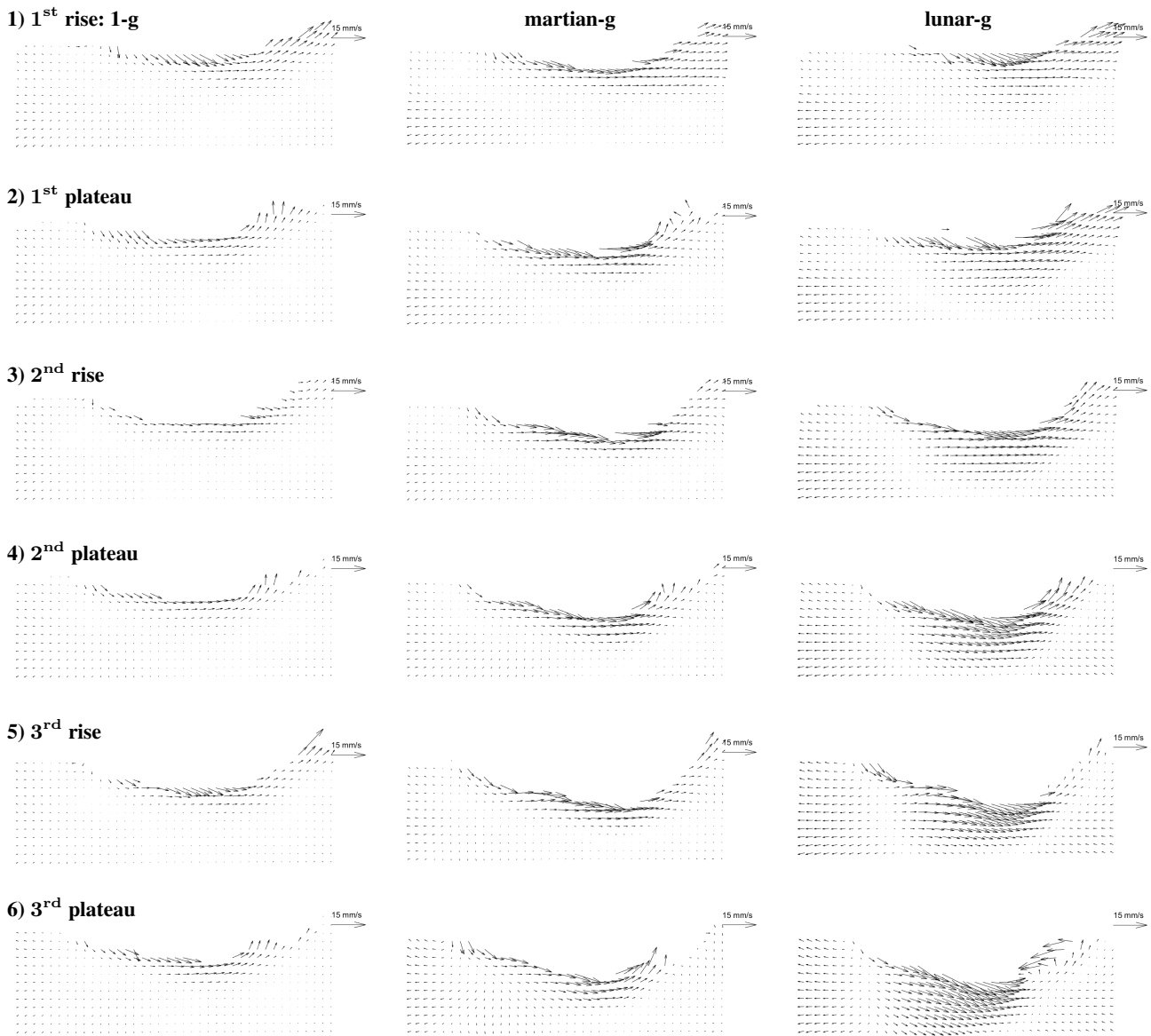


**Figure 18.** Velocity fields for, from left to right, tests in 1-g, martian-g, and lunar-g, at 70% slip and 164N wheel load, averaged over sinkage ‘rise’ and ‘plateau’ segments as demonstrated in Figure 9a. Arrows labelled 15 mm/s indicate magnitude of commanded rim speed.

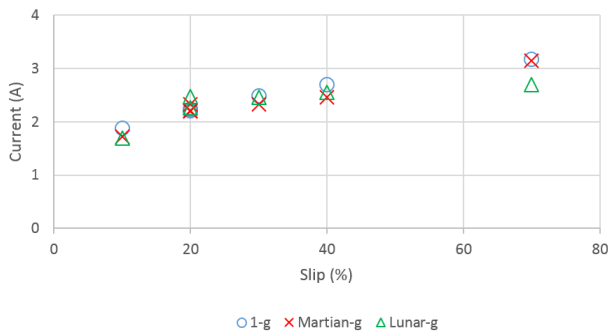


**Figure 19.** Average drive motor current versus slip ratio for tests in 1-g, martian-g, and lunar-g with wheel load setpoints of 164N.

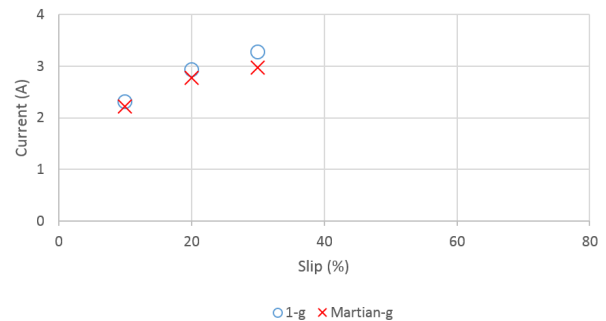


**Figure 20.** Average drive motor current versus slip ratio for tests in 1-g and martian-g with wheel load setpoints of 225N.

is observed in martian-g than in earth-g and, especially at high slip, even more is observed in lunar-g. More variation in

soil motion with respect to time is also observed in reduced-g than at 1-g. Analysis of the force data from the instrumented wheel experiments shows monotonically decreasing drawbar

pull as gravity is reduced. DP (at equal normal load and slip) is 8% lower on average in martian-g than in 1-g, and DP in lunar-g shows a statistically significant 20% reduction compared to 1-g. Sinkage is statistically significantly higher in reduced-g than in 1-g. All of these results are consistent with a weakening of soil strength in reduced gravity.

All of the above observations hinder a rover's ability to drive, and must be taken into consideration when interpreting results from mobility tests on Earth where only wheel load is reduced proportionally to the target reduction in gravity. The quantitative results suggest a starting point for factors of safety that could be applied when designing planetary rover wheels to meet minimum traction and/or maximum sinkage requirements.

New models and test methods should be developed that take into account the effect of reduced gravity on soil behaviour. Building up the experimental datasets further, with strategically selected wheels and soil simulants flown in reduced gravity using the apparatus described here, can build a foundation for future methods that more accurately predict robot mobility on extraterrestrial surfaces.

## Acknowledgements

This project was undertaken with the financial support of the Canadian Space Agency. The authors would like to thank Steeve Montminy and Francis Martin at the Canadian Space Agency for their project guidance and technical structural analysis guidance, respectively. We would like to thank Canada's National Research Council Flight Research Laboratory, especially Derek "Duff" Gowanlock, for facilitating the parabolic flight campaign. We thank Michel van Winnendael at the European Space Agency and Stéphane Michaud at RUAG Space for support regarding Martian soil simulants, and MDA for the loan of a prototype ExoMars rover wheel.

## References

- Alshibli KA, Batiste SN and Sture S (2003) Strain localization in sand: plane strain versus triaxial compression. *Journal of Geotechnical and Geoenvironmental Engineering* 129(6): 483–494.
- Arvidson R, Bell J, Bellutta P, Cabrol N, Catalano J, Cohen J, Crumpler L, Des Marais D, Estlin T, Farrand W, Gellert R, Grant J, Greenberger R, Guinness E, Herkenhoff K, Herman J, Iagnemma K, Johnson J, Klingelhöfer G, Li R, Lichtenberg K, Maxwell S, Ming D, Morriss R, Rice M, Ruff S, Shaw A, Siebach K, de Souza P, Stroupe A, Squyres S, Sullivan R, Talley K, Townsend J, Wang A, Wright J and Yen A (2010) Spirit mars rover mission: Overview and selected results from the northern home plate winter haven to the side of scamander crater. *Journal of Geophysical Research: Planets* 115(E7).
- Arvidson RE, Ashley JW, Bell J, Chojnacki M, Cohen J, Economou T, Farrand WH, Ferguson R, Fleischer I, Geissler P, Gellert R, Golombek M, Grotzinger J, Guinness E, Haberle R, Kerkenhoff K, Herman J, Iagnemma D, Jolliff B, Johnson J, Klingelhöfer G, Knoll A, Knudson A, Li R, McLennan S, Mittlefehldt D, Morriss R, Parker T, Rice M, Schröder C, Soderblom L, Squyres S, Sullivan R and Wolff M (2011) Opportunity mars rover mission: Overview and selected results from purgatory ripple to traverses to endeavour crater. *Journal of Geophysical Research: Planets* 116(E7).
- Arvidson RE, Iagnemma KD, Maimone M, Fraeman AA, Zhou F, Heverly MC, Bellutta P, Rubin D, Stein NT, Grotzinger JP and Vasavada AR (2017) Mars science laboratory curiosity rover megaripple crossings up to sol 710 in gale crater. *Journal of Field Robotics* 34(3): 495–518.
- Azimi A, Kövecses J and Angeles J (2013) Wheel–soil interaction model for rover simulation and analysis using elastoplasticity theory. *IEEE Transactions on robotics* 29(5): 1271–1288.
- Bekker MG (1956) *Theory of land locomotion*. Ann Arbor: University of Michigan Press.
- Boles W, Scott WD and Connolly JF (1997) Excavation forces in reduced gravity environment. *Journal of Aerospace Engineering* 10: 99–103.
- Brunskill C, Patel N, Gouache TP, Scott CM G P Saaj, Matthews M and Cui L (2011) Characterisation of martian soil simulants for the exomars rover testbed. *Journal of Terramechanics* 48(6): 419–438.
- Bui HH, Kobayashi T, Fukagawa R and Wells JC (2009) Numerical and experimental studies of gravity effect on the mechanism of lunar excavations. *Journal of Terramechanics* 46: 115–124.
- Callas JL (2015) Mars exploration rover spirit end of mission report. Technical report.
- Ding L, Deng Z, Gao H, Tao J, Iagnemma KD and Liu G (2015) Interaction mechanics model for rigid driving wheels of planetary rovers moving on sandy terrain with consideration of multiple physical effects. *Journal of Field Robotics* 32: 827–859.
- Edwards MB, Dewoolkar MM, Huston DR and Creager C (2017) Bevameter testing on simulant fillite for planetary rover mobility applications. *Journal of Terramechanics* 70: 13–26.
- Freitag D, Green A and Melzer K (1970) Performance evaluation of wheel for lunar vehicles. *Marshall Space Flight Center. National Aeronautics and Space Administration* : 1–53.
- Fujiwara A, Kawaguchi J, Yeomans D, Abe M, Mukai T, Okada T, Saito J, Yano H, Yoshikawa M and Scheeres D (2006) The rubble-pile asteroid itokawa as observed by hayabusa. *Science*

- 312: 1330–1334.
- Ghotbi B, Kovács L, González F, Niksirat P, Skonieczny K and Kövecses J (2018) Including the effect of gravity in wheel/terrain interaction models. In: *Proceedings of the in Proceedings of the 14th International Symposium on Artificial Intelligence, Robotics and Automation in Space (i-SAIRAS 2018)*.
- Heverly M, Matthews J, Lin J, Fuller D, Maimone M, Biesiadecki J and Leichty J (2013) Traverse performance characterization for the mars science laboratory rover. *Journal of Field Robotics* 30(6): 835–846.
- International Space Exploration Coordination Group (2018) Global exploration roadmap.
- Irani R, Bauer R and Warkentin A (2011) A dynamic terramechanic model for small lightweight vehicles with rigid wheels and grousers operating in sandy soil. *Journal of Terramechanics* 48: 307–318.
- Irani R, Bauer R and Warkentin A (2014) Application of a dynamic pressure-sinkage relationship for lightweight mobile robots. *International Journal of Vehicle Autonomous Systems* 12: 1–23.
- Jet Propulsion Laboratory, California Institute of Technology (2009) Second Test Rover Added to Driving Experiments. <https://www.jpl.nasa.gov/news/news.php?feature=2291>. Accessed: 2019-02-21.
- Kleinbans M, Markies H, De Vet S and Postema F (2011) Static and dynamic angles of repose in loose granular materials under reduced gravity. *Journal of Geophysical Research: Planets* 116(E11).
- Knuth MA, Johnson J, Hopkins M, Sullivan R and Moore J (2012) Discrete element modeling of a mars exploration rover wheel in granular material. *Journal of Terramechanics* 49(1): 27–36.
- Kobayashi T, Fujiwara Y, Yamakawa J, Yasufuku N and Omine K (2010) Mobility performance of a rigid wheel in low gravity environments. *Journal of Terramechanics* 47: 261–274.
- Lichtenheldt R, Burlet JY, Buse F and Rebele B (2017) Towards automated soil preparation for planetary rovers—methods for reproducible measurements in regolith simulants. In: *Symposium on Advanced Space Technologies in Robotics and Automation, ASTRA*. pp. 1–12.
- Lindemann RA and Voorhees CJ (2005) Mars exploration rover mobility assembly design, test and performance. In: *2005 IEEE International Conference on Systems, Man and Cybernetics*, volume 1. IEEE, pp. 450–455.
- Marshall JP, Hurley RC, Arthur D, Vlahinic I, Senatore C, Iagnemma K, Trease B and Andrade JE (2018) Failures in sand in reduced gravity environments. *Journal of the Mechanics and Physics of Solids* 113: 1–12.
- Meirion-Griffith G and Spenko M (2011) A modified pressure-sinkage model for small, rigid wheels on deformable terrains. *Journal of Terramechanics* 48: 149–155.
- Oravec H, Zeng X and Asnani V (2010) Design and characterization of grc-1: A soil for lunar terramechanics testing in earth-ambient conditions. *Journal of Terramechanics* 47(6): 361–377.
- Qian F, Daffon K, Zhang T and Goldman DI (2013) An automated system for systematic testing of locomotion on heterogeneous granular media. In: *Nature-Inspired Mobile Robotics*. World Scientific, pp. 547–554.
- Rothrock B, Papon J, Kennedy R, Ono M, Heverly M and Cunningham C (2016) Spoc: Deep learning-based terrain classification for mars rover missions. In: *AIAA SPACE 2016*. p. 5539.
- Rozitis B, MacLennan E and Emery JP (2014) Cohesive forces prevent the rotational breakup of rubble-pile asteroid (29075) 1950 da. *Nature* 512: 174.
- Senatore C and Iagnemma K (2014) Analysis of stress distributions under lightweight wheeled vehicles. *Journal of Terramechanics* 51: 1–17.
- Skonieczny K, Moreland S, Inotsume H, Wettergreen DS, Vivake M Asnani V and Creager C (2014) Visualizing and Analyzing Machine-soil Interactions using Computer Vision. *Journal of Field Robotics* 31: 753–769.
- Skonieczny K, Moreland SJ and Wettergreen DS (2012) A grouser spacing equation for determining appropriate geometry of planetary rover wheels. In: *2012 IEEE/RSJ International Conference on Intelligent Robots and Systems*. IEEE, pp. 5065–5070.
- Skonieczny K, Niksirat P and Nassiraei A (2019) Rapid automated soil preparation for testing planetary rover-soil interactions aboard reduced-gravity aircraft. *Journal of Terramechanics* 83: 35–44.
- Slonaker J, Motley DC, Zhang Q, Townsend S, Senatore C, Iagnemma K and Kamrin K (2017) General scaling relations for locomotion in granular media. *Physical Review E* 95(5): 052901.
- Wong J (1967) Behaviour of soil beneath rigid wheels. *Journal of Agricultural Engineering Research* 12: 257–269.
- Wong J (2012) Predicting the performances of rigid rover wheels on extraterrestrial surfaces based on test results obtained on earth. *Journal of Terramechanics* 49: 49–61.
- Wong JY and Reece A (1967) Prediction of rigid wheel performance based on the analysis of soil-wheel stresses part i. performance of driven rigid wheels. *Journal of Terramechanics* 4: 81–98.